Journal of Alloys and Compounds 915 (2022) 165366

Contents lists available at ScienceDirect

Journal of Alloys and Compounds

journal homepage: www.elsevier.com/locate/jalcom

High-entropy design and its influence on glass-forming ability in Zr–Cu-based metallic glass

Y. Ohashi[a], T. Wada[b,*], H. Kato[b]

[a] Department of Materials Science, Graduate School of Engineering, Tohoku University, Sendai 980-8579, Japan
[b] Institute for Materials Research, Tohoku University, Sendai 980-8577, Japan

ARTICLE INFO

Article history:
Received 14 June 2021
Received in revised form 22 April 2022
Accepted 7 May 2022
Available online 11 May 2022

Keywords:
Bulk metallic glass
High-entropy alloy
Glass-forming ability

ABSTRACT

The glass-forming ability of Zr–Cu-based metallic glass with high entropy is investigated. Samples are prepared by adding elements, such as Ag, Hf, and Ni, to ternary $Zr_{48}Al_7Cu_{45}$ to systematically evaluate the multicomponent effect. The glass structures are fabricated by tilt casting. In quaternary and senary alloys with increased glass-forming ability, new competitive liquid crystalline phases are generated with the addition of elements. Compared with the quaternary alloy, the quinary alloy does not form a new crystalline phase, and the added Hf is highly soluble in the base crystalline phase. The driving force for crystallization, which is evaluated based on specific heat measurements, is the largest for the quinary alloys. This suggests that stabilization of the competitive phase by the high-entropy effect leads to a decrease in the glass-forming ability. From the kinetics point of view, the relationship between the liquid-phase fragility and glass-forming ability is clarified, and the addition of Ag and Ni, which strengthens the liquid properties, is found to improve the glass-forming ability. Based on the high-entropy strategy, a new high-entropy metallic glass $Zr_{35}Hf_{13}Al_{11}Ag_8Ni_8Cu_{25}$, with a maximum vitrification diameter of 20 mm, is fabricated.

1. Introduction

ulk metallic glasses (BMGs) and high-entropy alloys (HEAs) are advanced materials that are currently attracting much attention in both the industrial and academic fields because of their various properties that differ from those of conventional alloys [1–4]. BMGs have no long-range structural periodicity in their atomic arrangement. They are generally obtained from freezing a disordered liquid structure below the glass transition temperature (T_g) and they crystallize via supercooled liquid when heated. Due to the uniformity of its long-range structure, BMGs generally exhibit excellent mechanical properties of high strength, high elastic limit, and low Young's modulus [5–7], and some Co-based BMGs, for example, exhibit high compressive yield stress of over 5000 MPa [8]. In addition, thermoplastic forming and blow molding using the viscous flow phenomenon in supercooled liquids are also possible. It thereby reduces the fabrication process and allows precise net-shape forming to be applied with nano-order and low processing stress [9,10].

EAs are crystalline alloys with equimolar compositions of five or more elements, which form a single-phase solid solution with a simple lattice such as face-centered cubic, body-centered cubic, or hexagonal close-packed structures. Four core effects, namely the high-entropy effect, sluggish diffusion effect, lattice distortion effect, and cocktail effect, have been proposed [11], and several HEAs with novel properties that cannot be obtained with conventional materials have been reported [12]. HEAs were first reported in 2004 [13,14] in a single-phase solid solution at exactly or near equimolar composition; however, the definition of HEAs was later broadened to include the number of constituent elements and compositional characteristics, regardless of whether the phase is single, multi, or amorphous, i.e., with five or more major elements with each element having a composition from 5% to 35%. Alternatively, HEAs can also be defined from the value of the configuration entropy S_{conf},

$$S_{conf} = -R\sum_{i=1}^{n} x_i \ln x_i, \quad (1)$$

where R is the gas constant (8.314 J/mol K), n is the number of components, and x_i is the mole fraction. Alloys with $1.5\,R < S_{conf}$ are regarded as HEAs, and currently this covers a wide range of alloys [15]. The S_{conf} corresponds to the number of possible atomic configurations and is regarded as a compositional complexity. A high S_{conf} of phase leads to a decrease in the Gibbs free energy of the

* Corresponding author.
E-mail address: wada-t@imr.tohoku.ac.jp (T. Wada).

https://doi.org/10.1016/j.jallcom.2022.165366
0925-8388/

phase, especially at high temperature, in comparison to the competing low temperature ordered intermetallic compound phase.

The Alloys that fit the definition of HEA and form amorphous solids on the order of mm or more are called high-entropy bulk metallic glasses (HE-BMGs). HE-BMGs are alloys that combine features of HEAs and BMGs; The core effects of HEA, such as high entropy and sluggish diffusion effects, effectively affect amorphous formation and relaxation properties, and it is expected to develop more thermally stable glass with superior formation ability. Some of the HE-BMGs reported so far have been found to exhibit suppression of softening near the glass transition temperature [16], increase in α-relaxation temperature confirmed by dynamic mechanical analysis [17], and an incubation time of 3600 s near the crystallization temperature [18]. Concerning the glass forming ability (GFA) of HE-BMGs, two conflicting effects have been pointed out so far [19]. The Adam-Gibbs theory [20], which links an increase in the configurational entropy of an alloy to a decrease in viscosity, promotes the mobility of the constituent elements and reduce their GFA. The confusion principle [21], on the other hand, supports the importance of compositional complexity for a high GFA; that is, a greater number of elements involved will lead to a lower chance that the alloy can select viable crystal structures and a greater chance of glass formation. The thermodynamic stability of the liquid phase is important for achieving high GFA of the alloy, and the increase in entropy of the liquid phase due to mixing elements is one of the factors that enhance it. Indeed, the GFA of an alloy has been increased by substituting the constituent elements of the prototypical BMG with an element from the same family or one close to it in the periodic table [22]. Such an approach has resulted in the development of compositionally complex ternary to quinary BMGs with high GFA on the centimeter scale.

o date, several HE-BMGs have been developed, mostly at or near equimolar composition. However, these equimolar HE-BMGs tend to exhibit lower GFA than the prototypical BMGs [23,24], which may arise from the discrepancy of the equimolar composition and eutectic composition in the multicomponent alloy. The eutectic composition is advantageous for glass formation from both thermodynamics and kinetics viewpoints because the liquid phase is in equilibrium only up to lower temperatures and the eutectic reaction requires fast kinetics to achieve long-range rearrangement of atoms. Recently, it has been shown that HE-BMGs tuned to non-equimolar eutectic compositions exhibit a high GFA [25]. However, the effect of increasing the components to the extent of high entropy on the GFA has not been studied systematically. In this work, we intend to clarify this by systematically increasing the number of components in the originally developed Zr–Cu-based multi-component alloy up to a senary system. The GFA and thermal properties of these eutectic alloys are examined and the effect of the number of components on the GFA is discussed from the thermodynamics and kinetics viewpoints.

2. Experimental

In this research, Zr–Cu-based ternary to senary eutectic compositions were used. Previously reported ternary and quaternary eutectic compositions of $Zr_{48}Al_7Cu_{45}$ and $Zr_{48}Al_8Cu_{36}Ag_8$ were employed without modification. The quinary and senary alloys were newly developed by adding Hf and Ni into $Zr_{48}Al_8Cu_{36}Ag_8$. Hf was chosen as a substitution for Zr because Hf has a zero heat of mixing with Zr and a near-zero atomic size difference (Zr: 0.162 nm, Hf: 0.160 nm). Ni was chosen as a substituent for Cu for similar reasons. The alloy with Ni and Hf added was tuned again to eutectic composition based on the result of thermal analysis and microstructural characterization. The alloys were prepared by arc-melting high-purity elements of Zr, Hf, Al, Ag, Cu, and Ni (purities of 99.9% or higher) under high-purity Ar gas. The alloy was arc-melted again on a water-cooled copper hearth under an Ar atmosphere, and the fully melted alloy was poured into a cylindrical copper mold connected to the copper hearth to produce rapidly quenched bulk samples. Heat treatment was performed by sealing specimens in a quartz tube under a vacuum of less than 5×10^{-3} Pa, and held at 1000 K, just below the melting point of the specimens, for 12 h using an electric furnace, which was followed by air cooling. The phase of the cast specimens was identified using X-ray diffractometers (D8ADVANCE, Bruker AXS Co (K_α), and Ultima IV, Rigaku, Cu-K_α line). For the evaluation of the GFA, molten alloy samples were poured into the cylindrical cavity of copper mold with different diameters of 8, 9, 10, 11, 12, 13, 14, 15, 20, 25 mm, and then the middle height of the cylindrical cast sample was cut into thin slices. After the surface was polished to remove impurities deposited during cutting, then X-rays were irradiated at the center of the sample. The microstructure and composition of the phase were analyzed by a scanning electron microscope (ULTRA55, Carl Zeiss) equipped with an energy-dispersive spectrometer (Nano GmbH, Bruker). Thermal analyses were performed using a differential thermal analyzer (SDT Q600, TA Instruments) to evaluate the solidification behavior. The temperature was raised above the melting temperature, then cooled to room temperature at a rate of 20 K/min under an Ar gas flow (200 mL/min). The glass transition temperature (T_g) and crystallization temperature (T_x) were measured using a differential scanning calorimeter (DSC8500, PerkinElmer) at a heating rate of 20 K/min. The heating rate dependence of the phase transition temperatures, T_g and T_x, was measured by changing the heating rate from 5 K/min to 140 K/min. The absolute specific heat capacity of the sample was calculated from the calorimetric curve obtained by measuring (i) an empty pan, (ii) a standard sample, and (iii) an unknown sample under the same conditions using the same apparatus. The unknown samples were measured on a glass sample and on a crystalline sample that had been raised to T_x and then cooled slowly. The empty pan was made of pure Al and the standard sample was made of sapphire. The measurement was carried out in a flowing Ar atmosphere with a flow rate of 100 mL/min. The heat flux measured by differential scanning calorimetry (DSC) is given by

$$\dot{Q} = \left(\frac{\partial Q}{\partial t}\right)_{\dot{T}\neq 0} - \left(\frac{\partial Q}{\partial t}\right)_{\dot{T}=0} = c\frac{dT}{dt}, \tag{2}$$

where $\left(\frac{\partial Q}{\partial t}\right)_{\dot{T}\neq 0}$ is the power required to heat the sample and empty pan at a constant heating rate, $\left(\frac{\partial Q}{\partial t}\right)_{\dot{T}=0}$ is the power required to maintain the sample and empty pan at a constant temperature, and c is the total heat capacity of the sample and empty pan. The temperature variation of the specific heat capacity of the sample is expressed by

$$C_p(T)_{\text{sample}} = \frac{\dot{Q}_{\text{sapphire}} - \dot{Q}_{\text{pan}}}{\dot{Q}_{\text{sapphire}} - \dot{Q}_{\text{pan}}} \frac{m_{\text{sapphire}}\mu_{\text{sample}}}{m_{\text{sample}}\mu_{\text{sapphire}}} C_p(T)_{\text{sapphire}}, \tag{3}$$

where m is the mass, μ is the molecular weight, and $C_p(T)_{\text{sapphire}}$ is the specific heat capacity of sapphire with reference to the literature value [26].

3. Results and Discussion

3.1. Optimizing multicomponent alloys to the eutectic composition

For the ternary and quaternary eutectic compositions, the previously reported $Zr_{48}Al_7Cu_{45}$ [27] and $Zr_{48}Al_8Cu_{36}Ag_8$ [28] were employed. The substitution of Zr with Hf in the $Zr_{48}Al_8Cu_{36}Ag_8$ alloy was tuned to the eutectic composition by the following process: First, thermal analyses on the alloys with different Hf contents was performed to find a composition that showed a single exothermic peak during solidification. Next the microstructure of the slowly solidified alloys was observed to determine whether a primary

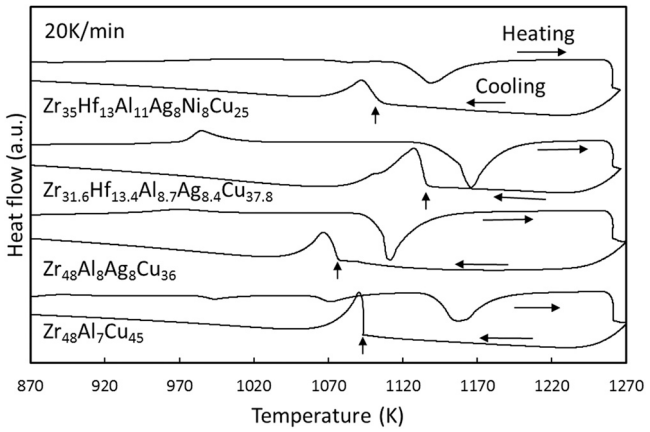

Fig. 1. Differential Thermal Analysis (DTA) measurement results for ternary to senary bulk metallic glass at a heating/cooling rate of 20 K/min. Arrows in the figure indicate the liquidus temperature (T_l).

crystal existed. Based on the compositional analysis on the primary crystal, the remaining eutectic liquid composition was estimated and an ingot of this composition was prepared. This series of analyses were repeated and finally the composition of $Zr_{31.6}Hf_{13.4}Al_{8.7}Cu_{37.8}Ag_{8.4}$ was found to be closest to the eutectic point. The addition of Ni to this quinary alloy and composition tuning by the above approach resulted in the senary eutectic composition of $Zr_{35}Hf_{13}Al_{11}Ag_8Ni_8Cu_{25}$. Fig. 1 shows the differential thermal analysis (DTA) measurement results for the ternary to senary eutectic alloys developed in this work. The endothermic peak during melting and the exothermic peak during solidification of all the alloys were approximately single, and there was no separate peak corresponding to the primary crystal on the high temperature side, which suggested that multiple phases precipitated simultaneously. Fig. 2(a)–(d) shows the microstructure, determined by DTA, of each alloy that was slowly solidified. Each sample showed fine eutectic lamellar; however, many primary crystals were observed in the ternary alloy. These thermal and microstructural analyses confirmed that the developed quinary and senary compositions were close to the eutectic. The eutectic structure of the quaternary and senary alloys formed a narrowly spaced phase. However, the quinary alloy formed broadly spaced phases.

3.2. Determination of GFA for the multicomponent eutectic alloys and its prediction with conventional thermo-parameters

The GFA of these eutectic alloys was examined by tilt casting the molten alloy into copper molds with a cylindrical cavity of different diameters. The representative results for the senary alloys are shown in Fig. 3(a). The X-ray diffraction (XRD) results of the 20-mm sample showed only a broad diffraction pattern and the outer appearance of the rod, shown in the inset of Fig. 3(a), shows a very smooth surface. These are typical characteristics of a glassy alloy. The XRD results of the 25-mm sample showed sharp peaks of the crystalline phase that overlapped with the broad diffraction peak of the glassy phase. Therefore, the maximum glass formation diameter (D_{max}) for the senary alloy was determined to be at least 20-mm. In the same way, the D_{max} of all ternary to senary alloys was examined and the results are shown with S_{conf} in Fig. 3(b). The D_{max} was highest in the quaternary alloy, decreased the most in the quinary alloy, then increased

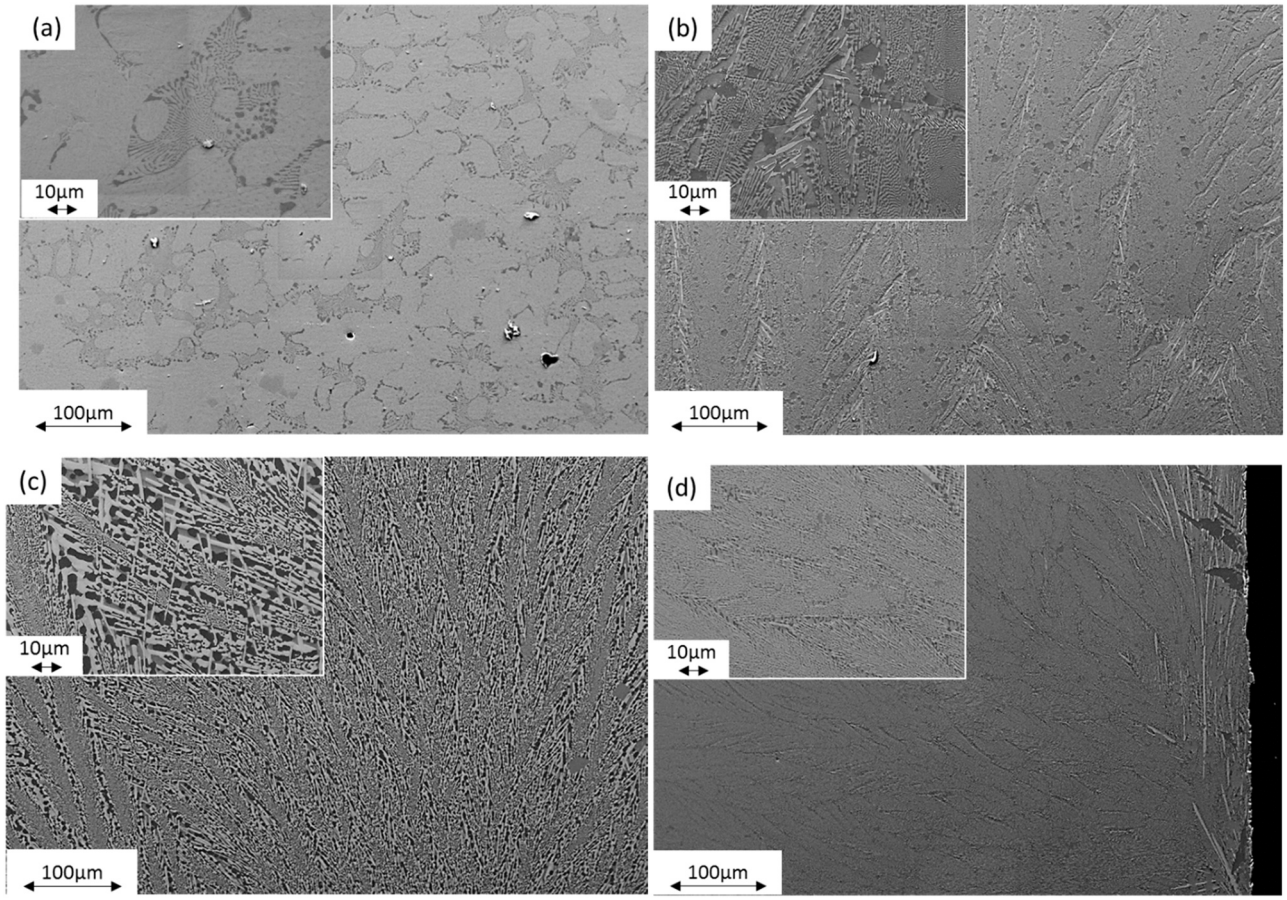

Fig. 2. Microstructure of each alloy slowly solidified by DTA: (a) ternary $Zr_{48}Al_7Cu_{45}$ alloy, (b) quaternary $Zr_{48}Al_8Ag_8Cu_{36}$ alloy, (c) quinary $Zr_{31.6}Hf_{13.4}Al_{8.7}Ag_{8.4}Cu_{37.8}$ alloy, and (d) senary $Zr_{35}Hf_{13}Al_{11}Ag_8Ni_8Cu_{25}$ alloy. Insets are enlarged pictures for each alloy.

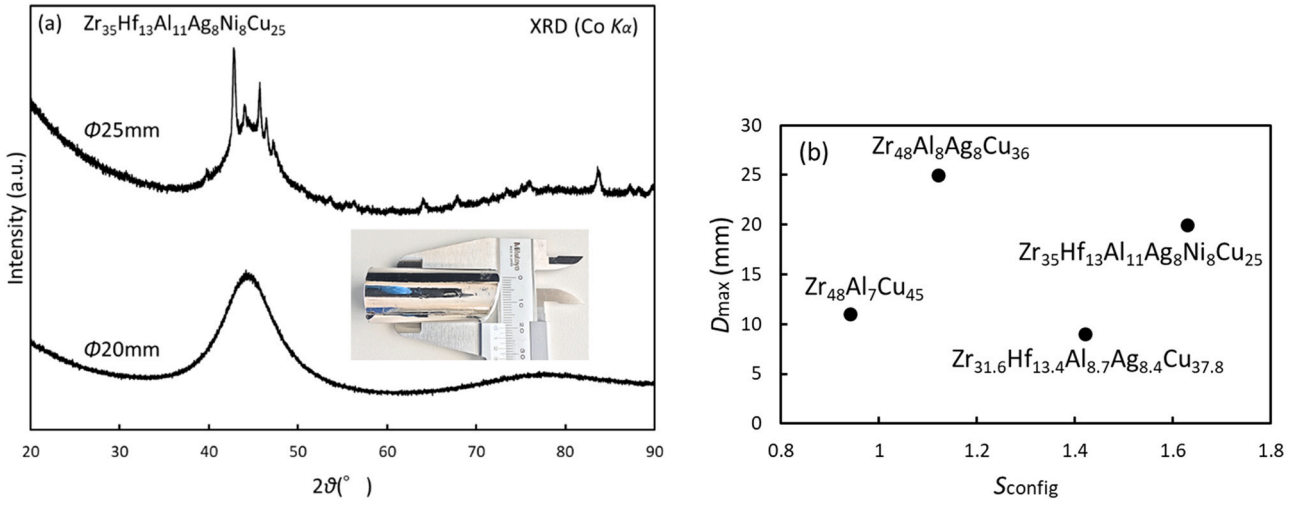

Fig. 3. (a) X-ray diffraction (XRD) evaluation of the maximum vitrification diameter (D_{max}) of a senary alloy ($Zr_{35}Hf_{13}Al_{11}Ag_8Ni_8Cu_{25}$). The inset shows the appearance of a 20-mm cast sample. (b) The maximum vitrification diameter (D_{max}) and the configuration entropy (S_{conf}) from Eq. (1) for each bulk metallic glass: ternary ($Zr_{48}Al_7Cu_{45}$ alloy), quaternary ($Zr_{48}Al_8Ag_8Cu_{36}$ alloy), quinary ($Zr_{31.6}Hf_{13.4}Al_{8.7}Ag_{8.4}Cu_{37.8}$ alloy), and senary ($Zr_{35}Hf_{13}Al_{11}Ag_8Ni_8Cu_{25}$ alloy).

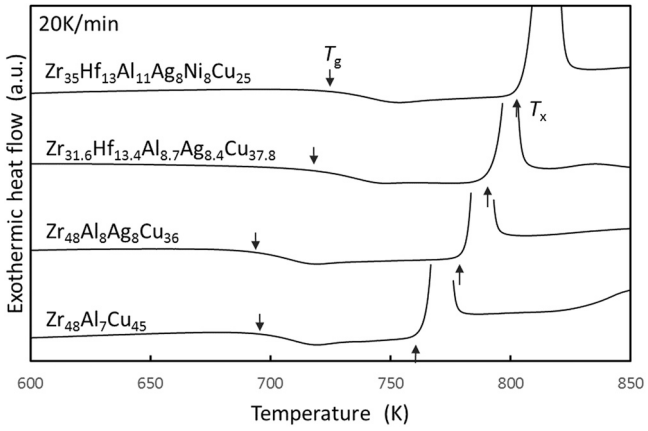

Fig. 4. DSC measurement results at a heating rate of 20 K/min for each bulk metallic glass.

again in the senary alloy. Fig. 4 shows the DSC measurement results at a heating rate of 20 K/min for each cast sample. A baseline shift indicating glass transition was confirmed in all samples, followed by crystallization. Table 1 summarizes T_g, T_x, liquidus temperature T_l, supercooled liquid region $\Delta T_x = T_x - T_g$, and reduced glass transition temperature $T_{rg} = T_g/T_l$ [29] measured by DSC and DTA at a heating or cooling rate of 20 K/min, together with the D_{max} and S_{conf} of each sample. Parameters for previously reported HE-BMGs are also shown together in the same Table 1 for comparison [25,30–33]. It has been reported that T_{rg} has good correlation with the GFA of conventional BMGs; however, our result was not consistent with this trend and the GFA of the alloy was almost independent of T_{rg}, especially in the quinary and senary alloys. Other reports have shown that T_{rg} does not predict the GFA for HE-BMGs. Thus, the inability of T_{rg} to accurately predict GFA may be common to HE-BMGs. However, ΔT_x, which indicates the stability of a supercooled liquid, showed a good correlation with D_{max} in the present work. The senary HE-BMG fabricated in this study has a configuration entropy comparable to that of quinary equimolar HE-BMGs, which is designed to have a off-eutectic composition to maximize the configuration entropy. On the other hand, D_{max} is larger than that of the equimolar composition alloys. The compatibility of high GFA and configuration entropy is due to the tuning of the multicomponent and eutectic compositions. The relatively high GFA is similar to other HE-BMGs tuned to eutectic composition. The D_{max} of the HE-BMG investigated in this study was the largest for a Be-free HE-BMG.

3.3. Competing crystalline counterparts generated in multicomponent eutectic alloys

To study the difference of equilibrium phases of these eutectic alloys, each glassy sample was encapsulated in a quartz tube under vacuum and annealed for 12 h at 1000 K, which is just below the solidus temperature of alloys. Fig. 5 shows the XRD results of the annealed samples of each alloy. The equilibrium phases of the ternary alloy ($Zr_{48}Al_7Cu_{45}$) were identified as the $CuZr_2$ ($C11_b$) and Cu_2ZrAl (L_21) phases. The equilibrium phases of the quaternary alloy ($Zr_{48}Al_8Cu_{36}Ag_8$) were almost the same as those of the ternary alloy but other peaks of ZrAg were newly detected, which indicated that the addition of Ag promoted the formation of a new compound phase. The equilibrium phases of the quinary alloy ($Zr_{31.6}Hf_{13.4}Al_{8.7}Cu_{37.8}Ag_{8.4}$) were the same as those of the quaternary alloy, which indicated the added Hf dissolved into any of the existing $CuZr_2$, Cu_2ZrAl, and ZrAg phases rather than forming a new phase. The equilibrium phases of the senary alloy ($Zr_{35}Hf_{13}Al_{11}Cu_{25}Ag_8Ni_8$) were almost the same as those of the quinary alloy, but the peaks from the CuZrAl phase were newly detected, which indicated that Ni addition promoted the formation of a new phase.

To confirm the above XRD results, DTA was used to analyze the composition of the phase in the slowly solidified microstructure (see Fig. 2(a)–(d) for the phase). Table 2 summarizes the results of the compositional analysis on the phases observed in the microstructure. The composition of the phases became more complex when the number of components increased but the elements with similar properties (e.g., Zr and Hf, Cu and Ni) merged. The composition of each phase was found to be expressed by the simple ratio among Zr, Al, Cu, and Ag groups and the compositions were almost coincident with those of the intermetallic phases identified by XRD in Fig. 5. Although the ZrCu phase could not be confirmed by XRD, the Zr–Al–Cu BMG was found to have metastable ZrCu (B2 phase) at high temperature [34], which is considered to be equivalent to ZrCu. It should be noted that Hf elements exist as a solute in the compound phases and no Hf-rich compound was observed in the quinary and senary alloys, which supports our discussion of the above XRD result.

Table 1
Configuration entropy from Eq. (1) (S_{conf}), maximum vitrification diameter (D_{max}), glass transition temperature (T_g), onset temperature of crystallization (T_x), liquidus temperature (T_l), and thermal parameters: thermal stability of the supercooled liquid state during heating ($\Delta T_x = T_x - T_g$) and the reduced glass transition temperature ($T_{rg} = T_g/T_l$) for alloys fabricated and referenced.

Alloys	S_{conf}/R	D_{max} (mm)	T_g (K)	T_x (K)	T_l (K)	ΔT_x	T_{rg}	composition	Ref
$Zr_{48}Al_7Cu_{45}$	0.94	11	695	759	1095	64	0.63	Eutectic	This work
$Zr_{48}Al_8Ag_8Cu_{36}$	1.12	25	694	777	1082	84	0.64	Eutectic	This work
$Zr_{31.6}Hf_{13.4}Al_{8.7}Ag_{8.4}Cu_{37.8}$	1.42	9	723	789	1144	66	0.63	Eutectic	This work
$Zr_{35}Hf_{13}Al_{11}Ag_8Ni_8Cu_{25}$	1.63	20	723	802	1112	79	0.65	Eutectic	This work
$Zr_{35}Hf_{17.5}Ti_{5.5}Al_{12.5}Co_{7.5}Ni_{12}Cu_{10}$	1.77	18	725	–	1206	–	0.60	Eutectic	[25]
$Pd_{20}Pt_{20}Ni_{20}Cu_{20}P_{20}$	1.61	10	580	645	820	65	0.71	Equimolar	[30]
$Ti_{20}Zr_{20}Hf_{20}Be_{20}Cu_{17.5}Ni_{12.5}$	1.74	30	632	684	1040	50	0.61	Eutectic	[31]
$Ti_{20}Zr_{20}Hf_{20}Cu_{20}Ni_{20}$	1.61	1.5	658	711	1149	53	0.57	Equimolar	[32]
$Ti_{20}Zr_{20}Cu_{20}Ni_{20}$ Be_{20}	1.61	3	691	732	1196	41	0.58	Equimolar	[33]

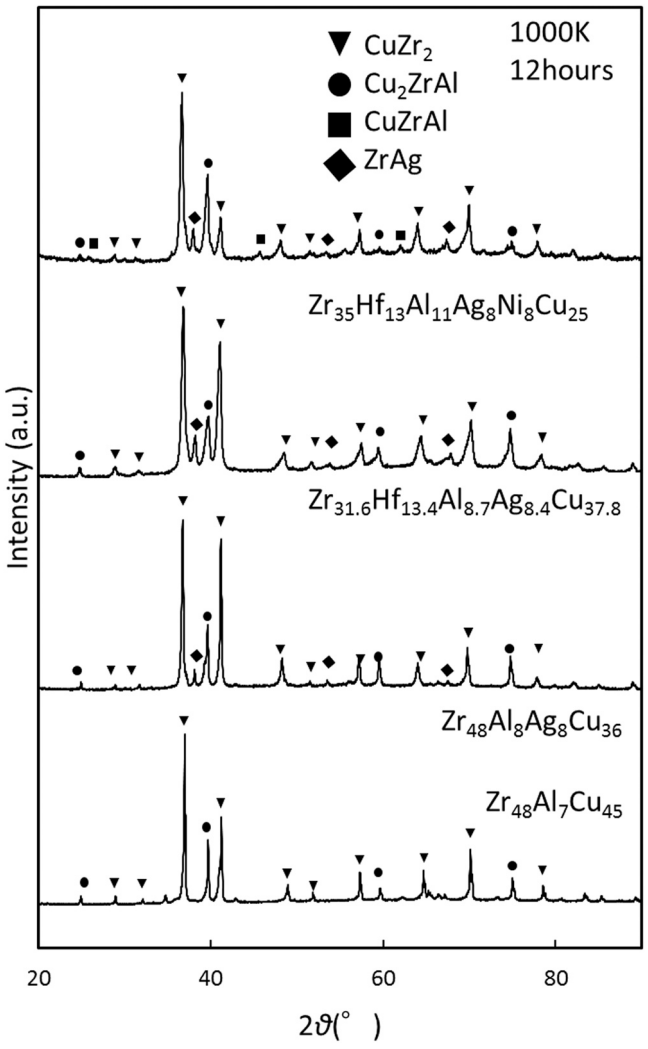

Fig. 5. XRD measurement results of ternary to senary vacuum heat-treated crystalline samples.

3.4. Thermodynamic driving force for eutectic reaction and its relation to GFA in multicomponent eutectic alloys

The free energy difference between the liquid and the competing crystal, ΔG^{l-x}, which corresponds to the driving force for the eutectic reaction, is a factor that has a significant effect on GFA. The free energy difference was experimentally determined by using DSC measurements with a sapphire standard sample. Fig. 6(a) shows the specific heat capacity of the supercooled liquid and crystallized state of each sample. Specific heat as a function of temperature was fit by Eqs. (4) and (5), for the liquid and crystalline phases, respectively [35,36].

$$C_p^l(T) = 3R + aT + bT^{-2}, \tag{4}$$

$$C_p^x(T) = 3R + cT + dT^2, \tag{5}$$

where $C_p^l(T)$ is the specific heat capacity of the supercooled liquid, $C_p^x(T)$ is the specific heat capacity of the crystal, and a, b, c, and d are the fitting parameters. Table 3 shows the values of the parameters obtained by the fitting, together with the enthalpy (H_f) and entropy fusion ($S_f = H_f/T$) measured by DSC. The specific heat capacity difference between the supercooled liquid and the crystal is expressed by

Table 2
Results of composition analysis (at%) of slowly cooled solidification phases of bulk metallic glasses: (a) ternary $Zr_{48}Al_7Cu_{45}$ alloy, (b) quaternary $Zr_{48}Al_8Ag_8Cu_{36}$ alloy, (c) quinary $Zr_{31.6}Hf_{13.4}Al_{8.7}Ag_{8.4}Cu_{37.8}$ alloy, and (d) senary $Zr_{35}Hf_{13}Al_{11}Ag_8Ni_8Cu_{25}$ alloy.

(a) Ternary. White (Contrast of SEM images)	**Zr**	**Al**	**Cu**
at%	66.5	1.4	32.1
Composition		$Zr_{66.5}(Al,Cu)_{33.5}$	
Structure		$CuZr_2(C11_b)$	
Gray	**Zr**	**Al**	**Cu**
at%	51.4	4.0	44.6
Composition		$Zr_{51.4}(Al,Cu)_{48.6}$	
Structure		$ZrCu(B_2)$	
Black	**Zr**	**Al**	**Cu**
at%	26.3	20.3	53.4
Composition		$Cu_{53.4}Zr_{26.3}Al_{20.3}$	
Structure		$Cu_2ZrAl(L2_1)$	

(b) Quaternary. White	**Zr**	**Al**	**Ag**	**Cu**
at%	65.7	1.4	10.9	22
Composition			$Zr_{65.7}(Al,Ag,Cu)_{34.3}$	
Structure			$CuZr_2(C11_b)$	
Gray(minor)	**Zr**	**Al**	**Ag**	**Cu**
at%	48.8	3.6	4.0	43.6
Composition			$Zr_{48.8}(Al,Ag,Cu)_{51.3}$	
Structure			$ZrCu(B_2)$	
Black	**Zr**	**Al**	**Ag**	**Cu**
at%	25.6	17.1	6.5	50.8
Composition			$Zr_{25.6}(Al,Ag)_{23.6}Cu_{50.8}$	
Structure			$Cu_2ZrAl(L2_1)$	

(c) Quinary. White	**Zr**	**Hf**	**Al**	**Ag**	**Cu**
at%	31.6	34.8	0	4.7	28.9
Composition			$(Zr,Hf)_{66.4}(Ag,Cu)_{33.6}$		
Structure			$CuZr_2(C11_b)$		
Gray(minor)	**Zr**	**Hf**	**Al**	**Ag**	**Cu**
at%	26.5	16.9	0.4	4.5	51.6
Composition			$(Zr,Hf)_{43.3}(Al,Ag,Cu)_{56.6}$		
Structure			$ZrCu(B_2)$		
Black	**Zr**	**Hf**	**Al**	**Ag**	**Cu**
at%	19.6	6.0	17.3	4.7	52.4
Composition			$(Zr,Hf)_{25.3}(Al,Ag)_{22}Cu_{52.4}$		
Structure			$Cu_2ZrAl(L2_1)$		

(d) Senary. White	**Zr**	**Hf**	**Al**	**Ag**	**Ni**	**Cu**
at%	45	19.9	2.4	9	3.2	20.6
Composition			$(Zr,Hf)_{65}(Al,Ag,Ni,Cu)_{35}$			
Structure			$CuZr_2(C11_b)$			
Gray	**Zr**	**Hf**	**Al**	**Ag**	**Ni**	**Cu**
at%	30.5	12.3	6.6	5.6	14.5	30.5
Composition			$(Zr,Hf,Ag)_{48.4}(Al,Ni,Cu)51.6$			
Structure			$ZrCu(B_2)$			
Black	**Zr**	**Hf**	**Al**	**Ag**	**Ni**	**Cu**
at%	31	7.3	26.2	3.7	4.6	24
Composition			$(Zr,Hf)_{38.3}(Ag,Cu)_{29.8}(Ni,Cu)_{28.6}$			
Structure			ZrAlCu			

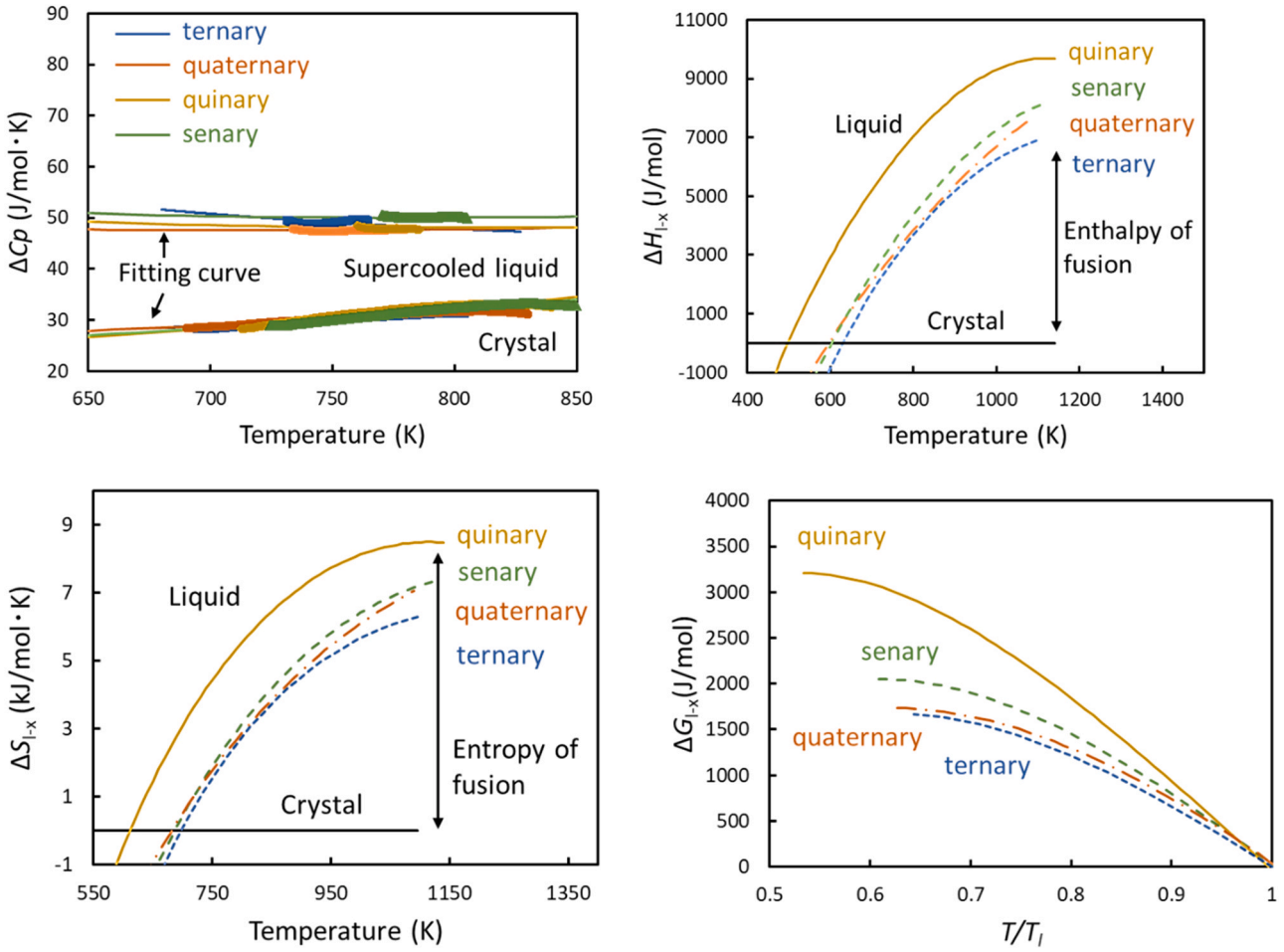

Fig. 6. (a) Specific heat capacity measurement results of each sample. (b) The temperature change of the enthalpy difference between liquid and crystal. (c) The temperature change of the entropy difference between liquid and crystal. (d) The temperature change of the Gibbs free energy difference between liquid and crystal. Temperature (T) is normalized by the liquidus temperature (T_l).

$$\Delta C_p^{l-x}\ (T) = C_p^l(T) - C_p^x(T) \tag{6}$$

The enthalpy difference between the supercooled liquid and the crystal is derived by Eq. (7) and the entropy difference by Eq. (8).

$$\Delta H^{l-x}(T) = \Delta H_f - \int_T^{T_f} \Delta C_p^{l-x}(T')dT', \tag{7}$$

$$\Delta S^{l-x}(T) = \frac{\Delta H_f}{T_f} - \int_T^{T_f} \frac{\Delta C_p^{l-x}(T')}{T'}dT' \tag{8}$$

Although T_f denotes melting point, in this experiment T_l was used. Fig. 6(b) shows the temperature dependence of $\Delta H^{l-x}(T)$ for each sample. Similarly, Fig. 6(c) shows the temperature dependence of $\Delta S^{l-x}(T)$. Using $\Delta H^{l-x}(T)$ and $\Delta S^{l-x}(T)$, the temperature change of the Gibbs free energy difference between the supercooled liquid and the crystal can be obtained from

$$\Delta G^{l-x}\ (T) = \Delta H^{l-x}(T) - T\Delta S^{l-x}(T). \tag{9}$$

The calculated $\Delta G^{l-x}(T)$ as a function of temperature normalized by individual T_l is shown in Fig. 6(d). The $\Delta G^{l-x}(T)$ and the GFA of each sample were roughly correlated, and the quinary alloy with the lowest D_{max} was confirmed to have a high driving force for the eutectic reaction.

3.5. Why does the high entropy design not always decrease the driving force for eutectic reaction?

Correlating the change in the GFA of the alloys (Fig. 3(b)) with the difference in the crystalline phases (Fig. 5), there seems to be a relationship between the GFA and the formation of new phase by an additional element; that is, the GFA increases when the additional element (Ag, Ni) forms a new phase, and when the additional element (Hf) dissolves in the existing phase, the GFA decreases.

Table 3
Fitting parameters (a–d), liquidus temperature (T_l), enthalpy of fusion (ΔH_f), and entropy of fusion (ΔS_f) of each bulk metallic glass.

Composition	$Zr_{48}Al_7Cu_{45}$	$Zr_{48}Al_8Ag_8Cu_{36}$	$Zr_{31.6}Hf_{13.4}Al_{8.7}Ag_{8.4}Cu_{37.8}$	$Zr_{35}Hf_{13}Al_{11}Ag_8Ni_8Cu_{25}$
a(J mol^{-1}K^{-2})	0.0118	0.0210	0.0190	0.0215
b(J mol^{-1}K^{-3})	8,620,000	3.858,000	5,048,000	5,124,000
c(J mol^{-1}K^{-2})	-0.0096	-0.0110	-0.0258	-0.0213
d(J mol^{-1}K^{-2})	2.2×10^{-5}	2.4×10^{-5}	4.3×10^{-5}	3.8×10^{-5}
T_f(K)	1095	1085	1144	1117
ΔH_f(kJ mol^{-1})	6.9	7.7	9.7	8.2
ΔS_f(J mol^{-1}K^{-1})	6.3	7.1	8.5	7.3

We discuss such a tendency of the GFA of the alloys from the viewpoint of the configuration entropy on the crystalline phase. By increasing the number of components, the compositional complexity leads to a decreased free energy of the liquid phase owing to the high configuration entropy, and this should result in the decrease of ΔG^{l-x} if the free energy of the competing crystal phases is unchanged. However, as evidenced by the XRD and compositional analyses, the additional element resulted in either new phase formation or dissolution in the existing phase, which should affect the free energy of the competing crystal phases. Here, we estimate the effect of dissolution of an element on the configuration entropy of the intermetallic phase, using a sublattice model [37]. The configuration entropy of an intermetallic compound in the ideal solution $S^{IM,ideal}$ is expressed by

$$S^{IM,ideal} = -R\left(\frac{\sum_{x=1}^{x} a^x \sum_{i=1}^{N} f_i^x \ln(f_i^x)}{\sum_{x=1}^{x} a^x}\right), \quad (12)$$

where a^x is the number of sites in the sub-lattice, f_i^x is the ratio of elements (numbered by i) in the sites, and N is the total number of elements. Using this model, we estimated the configuration entropy of the $CuZr_2$ phase in the quaternary and quinary alloys with their compositions shown in Table 2 (b) and (c). For simplicity, it was assumed that Hf occupies the Zr site and Al and Ag occupy the Cu site with a probability proportional to the composition of each element. The calculated configuration entropies of the $CuZr_2$ phase are 0.26 R and 0.6 R, respectively, for the quaternary and quinary alloys (the difference is 0.34 R). The configuration entropy difference between the quaternary and quinary liquid phases is 0.3 R. That is, when Hf is added, the increase in entropy that contributes to the stability of the phase is more remarkable in the competitive crystal phase than in the liquid phase. Hf exhibited good compatibility with Zr, namely, Hf could substitute in Zr sites in large amounts because of the almost identical atomic size and 0 kJ/mol for the heat of mixing with Zr. Therefore, addition of Hf resulted in its dissolution in the existing crystal phases and such a compositionally complex intermetallic phase, namely, high-entropy inter-metallics, increases the configuration entropy of the phase, hence the stability of the competing crystalline phase also increased, which did not result in the reduction of ΔG^{l-x}.

In contrast, the atomic size difference between Ag (0.144 nm) and Cu (0.128 nm) is relatively large and the heat of mixing between Ag and Cu is + 2 kJ/mol. From the phase diagram, the solid solubility is limited, and no intermetallic compound is seen, which indicates a low compatibility of Ag with Cu. The addition of Ag in the Zr–Al–Cu ternary alloy resulted in the formation of different crystal phases rather than forming a substituted solid solution with Cu. In this case, the configuration entropy of the compound phase remained negligible and the stability of the competing crystalline phase was almost unchanged, which resulted in the reduction of ΔG^{l-x}.

For alloys with few components, it is easy to find an element distinct from the existing one that does not dissolve into the existing phase. However, in the cases of quinary, senary, septenary and even more components, where they are categorized as a high-entropy material, because the alloy already contains elements with a variety of atomic sizes and interatomic interactions, it becomes more difficult to find another element that is distinct from the existing elements. Thus, the additional element has more possibility to dissolve into the existing phase. Cantor also reported similar results where alloys with many components are composed of far fewer phases than what is allowed by the Gibbs phase rule, probably owing to the inter-solid solubility and the absence of a multicomponent compound phase [13]. This might be one reason for the lower GFA of HE-BMGs than expected.

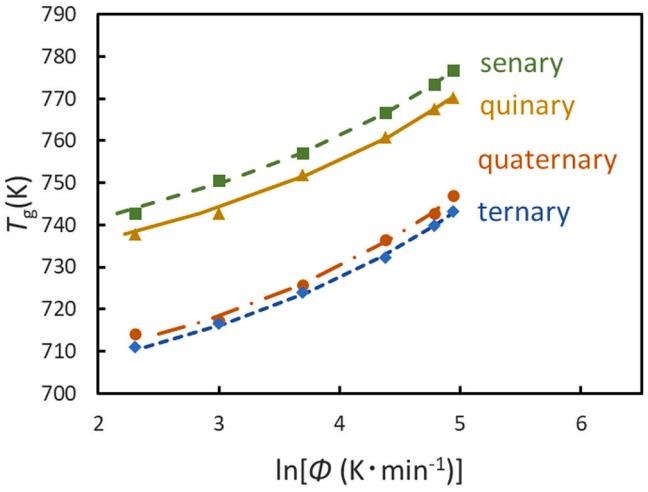

Fig. 7. Dependence of the glass transition temperature on the heating rate (plots) of each sample and VFT fitting curve.

3.6. Considering GFA of multicomponent eutectic alloy from thermodynamic and kinetic viewpoints

Kinetically, the viscosity of an alloy is an important parameter affecting its GFA, as well as the thermodynamic driving force for the eutectic reaction. The viscosity coefficient is inversely related to the diffusion coefficient of the elements by the Stokes–Einstein equation and it is considered that greater viscosity will lead to slower crystallization and more difficult glass formation [29,38,39]. Liquid is classified into strong or fragile by the slope of the temperature dependence of viscosity near T_g [40]. In a strong liquid, viscosity follows an Arrhenius-type relation, while in a fragile liquid, the viscosity deviates from the Arrhenius-type relation and remains lower than the melting temperature but sharply increases when approaching T_g. Metallic glasses generally exhibit properties intermediate between those of strong and fragile liquids [41]. The fragility of a liquid can be estimated from the dependence of T_g on the heating rate, which is expressed by the Vogel–Fulcher–Tammann (VFT)-type equation, Eq. (10) [42].

$$\phi(T_g) = B\exp\left[\frac{D^* T_g^0}{T_g^0 - T_g}\right], \quad (10)$$

where Φ is the heating rate [K/min], B is a constant, $T_g{}^0$ is the VFT temperature, and D^* is the intensity parameter. Additionally, the fragility index m is calculated using Eq. (11) [40].

$$m = \frac{D^* T_0 T_g}{(T_g - T_0)^2 ln10} \quad (11)$$

Fig. 7 shows the dependence of T_g on the heating rate for each glass sample measured by DSC and the fitted curves obtained by the VFT method. The fragility index m of each glass sample obtained by this fitting is shown in Table 4 together with the B, $T_g{}^0$, and D^* values. Table 4 also includes the values of the references and their respective maximum vitrification diameters [43–45]. The fragility index of the quaternary alloys is estimated to be 38, while that of the quinary and senary alloys is 44. The fragile behavior of the liquid means that the atoms in the supercooled liquid can diffuse more easily, which has a negative effect kinetically on the GFA by promoting crystal growth. The quinary alloy has the largest driving force for the eutectic reaction and the largest fragility index, and therefore, the smallest GFA among the three alloys. In contrast, the GFA of the quaternary alloy is the largest because it has both a smaller driving force for the eutectic reaction and the smallest fragility index among the three alloys. As

Table 4
Fitting parameters (B, T_g^0, D^*) and fragility index (m) of each bulk metallic glass.

Composition	$Zr_{48}Al_7Cu_{45}$	$Zr_{48}Al_8Ag_8Cu_{36}$	$Zr_{31.6}Hf_{13.4}Al_{8.7}Ag_{8.4}Cu_{37.8}$	$Zr_{35}Hf_{13}Al_{11}Ag_8Ni_8Cu_{25}$
B	8.43×10^3	5.68×10^3	9.08×10^3	9.2×10^3
T_g^0	659	665	688	692
D^*	0.159	0.458	0.500	0.509
m	40	38	44	44

Composition	$B \times 10^3$	T_g^0	D^*	m	D_{max}	Ref
$Zr_{48}Al_7Cu_{45}$	8.43	659	0.159	40	11	This work
$Zr_{48}Al_8Ag_8Cu_{36}$	5.68	665	0.458	38	25	This work
$Zr_{31.6}Hf_{13.4}Al_{8.7}Ag_{8.4}Cu_{37.8}$	9.08	688	0.500	44	9	This work
$Zr_{35}Hf_{13}Al_{11}Ag_8Ni_8Cu_{25}$	9.20	692	0.509	44	20	This work
$Zr_{33}Hf_8Ti_6Cu_{32}Ni_{10}Co_5Al_6$	–	–	–	42	> 2	[43]
$Ti_{16.7}Zr_{16.7}Hf_{16.7}Cu_{16.7}Ni_{16.7}Be_{16.7}$	–	–	–	33	15	[44]
$Ti_{32.8}Zr_{30.2}Ni_{5.3}Cu_9Be_{22.7}$	–	–	–	26	50	[45]

can be seen from Table 4, the increase of fragility with alloy multiplicity is consistent with previous studies dealing with Zr-Cu-based HE-BMG. On the other hand, several HE-BMGs with strong behavior were identified in the Zr-Be-based, indicating that the configuration entropy of the alloy is not always related to the fragility index. Clarifying the relationship between these parameters is important from the viewpoint of controlling the properties of metallic glasses and is a subject for future work.

4. Conclusions

High-entropy bulk metallic glass (HE-BMG) is considered to have a superior GFA compared with existing BMGs owing to the entropy stabilization of the supercooled liquid phase by compositional complexity. We clarified this by systematically increasing the number of components in the originally developed Zr–Cu-based multicomponent eutectic alloys from ternary ($n = 3$) to senary ($n = 6$) systems. We then discussed the results from thermodynamic and kinetic viewpoints.

1. Increasing the number of components (n) in Zr–Cu-based eutectic alloys, e.g., $Zr_{48}Al_7Cu_{45}$ ($n = 3$, D_{max} = 11 mm), $Zr_{48}Al_8Ag_8Cu_{36}$ ($n = 4$, D_{max} = 25 mm), $Zr_{31.6}Hf_{13.4}Al_{8.7}Ag_{8.4}Cu_{37.8}$ ($n = 5$, D_{max} = 9 mm), and $Zr_{35}Hf_{13}Al_{11}Ag_8Ni_8Cu_{25}$ ($n = 6$, D_{max} = 20), does not result in increasing the GFA.
2. A clear tendency exists where the GFA of the alloy decreases when the additive element is solidly dissolved into the original competitive crystalline phase. This is because of the thermodynamical stabilization of the resulting dissolved crystalline phase from the increased configurational entropy, which results in increasing the driving force of the eutectic reaction. In contrast, the GFA of the alloy increases when the additive element creates a new crystalline phase.
3. Ag and Ni have larger differences in atomic size and chemical interactions with other elements compared with the substitution source, Cu. The addition of Ag and Ni forms a new phase, and thus enhances the GFA in a Zr-Cu-based eutectic alloy. However, Hf has a smaller difference in atomic size from the substitution source, Zr, and a smaller heat of mixing difference from the constituent elements, so the Hf additive tends to replace Zr sites in the original crystalline phase, thus degrading the GFA.
4. The GFA of the Zr–Cu-based multicomponent eutectic alloys can be understood using both thermodynamic and kinetic parameters, e.g., the $Zr_{48}Al_8Ag_8Cu_{36}$ quaternary alloy with the largest GFA bears both a smaller driving force for the eutectic reaction and the smallest fragility parameter (m = 38). In contrast, the $Zr_{31.6}Hf_{13.4}Al_{8.7}Ag_{8.4}Cu_{37.8}$ quinary alloy with the smallest GFA bears the largest driving force for the eutectic reaction and the largest fragility parameter (m = 44).

CRediT authorship contribution statement

Yusuke Ohashi: Investigation, Methodology, Formal analysis, Data curation, Writing – original draft. **Takeshi Wada**: Conceptualization, Resources, Investigation, Methodology, Writing – review & editing. **Hidemi Kato**: Writing – review & editing, Supervision, Funding acquisition.

Declaration of Competing Interest

The authors declare that they have no known competing financial interests or personal relationships that could have appeared to influence the work reported in this paper.

Acknowledgment

This work was supported by a Grant-in-Aid for Scientific Research on the innovation area “Science of New-Class of Materials Based on Elemental Multiplicity and Heterogeneity (Grant No. 18H05452)” from the Ministry of Education, Culture, Sports, Science and Technology (MEXT) of Japan. We thank Edanz (https://jp.edanz.com/ac) for editing a draft of this manuscript.

References

[1] D.B. Miracle, O.N. Senkov, A critical review of high entropy alloys and related concepts, Acta Mater. 122 (2017) 488–511, https://doi.org/10.1016/j.actamat.2016.08.081
[2] B. Cantor, Multicomponent high-entropy Cantor alloys, Prog. Mater. Sci. 13 (2020) 100754, https://doi.org/10.3390/e16094749
[3] A. Inoue, Stabilization of metallic supercooled liquid and bulk amorphous alloys, Acta Mater. 48 (2000) 279–306, https://doi.org/10.1016/S1359-6454(99)00300-6
[4] Y.F. Ye, Q. Wang, J. Lu, C.T. Liu, Y. Yang, The generalized thermodynamic rule for phase selection in multicomponent alloys, Intermetallics 59 (2015) 75–80, https://doi.org/10.1016/j.intermet.2014.12.011
[5] M. Telford, The case for bulk metallic glass, Mater. Today 7 (2004) 36–43, https://doi.org/10.1016/S1369-7021(04)00124-5
[6] W.H. Wang, C. Dong, C.H. Shek, Bulk metallic glasses, Mater. Sci. Eng. R 44 (2004) 45–89, https://doi.org/10.1016/j.mser.2004.03.001
[7] J.F. Loffler, Bulk metallic glasses, Intermetallics 11 (2003) 529–540, https://doi.org/10.1016/S0966-9795(03)00046-3
[8] Z. Tao, Y. Qin, J. YunFei, L. Ran, P. ShuJie, W. JianFeng, X. Tao, Centimeter-scale-diameter Co-based bulk metallic glasses with fracture strength exceeding 5000MPa, Chin. Sci. Bull. 56 (2011) 3972–3977, https://doi.org/10.1007/s11434-011-4765-8
[9] J. Schroers, On the formability of bulk metallic glass in its supercooled liquid state, Acta Mater. 56 (2008) 471–478, https://doi.org/10.1016/j.actamat.2007.10.008

[10] J. Schroers, Processing of Bulk metallic Glass, Adv. Mater. 22 (2010) 1566–1597, https://doi.org/10.1002/adma.200902776
[11] M.H. Tsai, J.W. Yeh, High-entropy alloys: a critical review, Mater. Res. Lett. 3 (2014) 107–123, https://doi.org/10.1080/21663831.2014.912690
[12] O.N. Senkov, J.M. Scott, S.V. Senkova, D.B. Miracle, C.F. Woodward, Microstructure and room temperature properties of a high-entropy TaNbHfZrTi alloy, J. Alloy. Compd. 509 (2011) 6043–6048, https://doi.org/10.1016/j.jallcom.2011.02.171
[13] B. Cantor, I.T.H. Chang, P. Knight, A.J.B. Vincent, Microstructural development in equiatomic multicomponent alloys, Mater. Sci. Eng. A 375–377 (2004) 213–218, https://doi.org/10.1016/j.msea.2003.10.257
[14] J.W. Yeh, S.K. Chen, S.J. Lin, J.Y. Gan, T.S. Chin, T.T. Shun, C.H. Tsau, S.Y. Chang, Nanostructured high-entropy alloys with multiple principal elements: novel alloy design concepts and outcomes, Adv. Eng. Mater. 6 (2004) 299–303, https://doi.org/10.1002/adem.200300567
[15] M.C. Gao, J.W. Yeh, P.K. Liaw, Y. Zhang, "High-Entropy Alloys, Fundamental and Applications, 1st ed." Springer, 2016.
[16] Q. Zhou, Y. Du, Q. Jia, W. Han, X. Zhao, Y. Deng, H. Wang, A nanoindentation study of Ti-based high entropy bulk metallic glasses at elevated temperatures, J. Non Cryst. Solids 532 (2020) 119878, https://doi.org/10.1016/j.jnoncrysol.2019.119878
[17] J. Jiang, Z. Lu, J. Shen, T. Wada, H. Kato, M. Chen, Decoupling between calorimetric and dynamical glass transitions in high-entropy metallic glasses, Nat. Commun. 12 (2021) 3843, https://doi.org/10.1038/s41467-021-24093-w
[18] A. Inoue, Z. Wang, D.V. Louzguine-Luzgin, Y. Han, F.L. Kong, E. Shalaan, F. Al-Marzouki, Effect of high-order multicomponent on formation and properties of Zr-based bulk glassy alloys, J. Alloy. Compd. 638 (2015) 197–203, https://doi.org/10.1016/j.jallcom.2015.03.078
[19] J. Kim, H.S. Oh, J. Kim, C.W. Ryu, G.W. Lee, H.J. Chang, E.S. Park, Utilization of high entropy alloy characteristics in Er-Gd-Y-Al-Co high entropy bulk metallic glass, Acta Mater. 155 (2018) 350–361, https://doi.org/10.1016/j.actamat.2018.06.024
[20] G. Adam, J.H. Gibbs, On the temperature dependence of cooperative relaxation properties in glass-forming liquids, L. Chem. Phys. 43 (1965) 139–146, https://doi.org/10.1063/1.1696442
[21] A.L. Greer, Confusion by design, Nature 366 (1993) 303, https://doi.org/10.1038/366303a0
[22] A. Inoue, N. Nishiyama, Extremely low critical cooling rates of new Pd-Cu-P base amorphous alloys, Mater. Sci. Eng. A 226–228 (1997) 401–405, https://doi.org/10.1016/S0921-5093(97)80051-2
[23] H.Y. Ding, K.F. Yao, High entropy Ti20Zr20Cu20Ni20Be20 bulk metallic glass, J. Non Cryst. Solids 364 (2013) 9–12, https://doi.org/10.1016/j.jnoncrysol.2013.01.022
[24] M. Yang, X.J. Liu, H.H. Ruan, Y. Wu, H. Wang, Z.P. Lu, High thermal stability and sluggish crystallization kinetics of high-entropy bulk metallic glasses, J. Appl. Phys. 199 (2016) 245112, https://doi.org/10.1063/1.4955060
[25] T. Wada, J. Jiang, K. Yubuta, H. Kato, A. Takeuchi, Septenary Zr-Hf-Ti-Al-Co-Ni-Cu high-entropy bulk metallic glasses with centimeter-scale GFA, Materialia 7 (2019) 100372, https://doi.org/10.1016/j.mtla.2019.100372
[26] TA instruments, ⟨http://www.tainst.com⟩.
[27] D. Wang, H. Tan, Y. Li, Multiple maxima of GFA in three adjacent eutectics in Zr-Cu-Al alloy system – A metallographic way to pinpoint the best glass forming alloys, Acta Mater. 53 (2005) 2969–2979, https://doi.org/10.1016/j.actamat.2005.03.012
[28] W. Zhang, Q. Zhang, C. Qin, A. Inoue, Synthesis and properties of Cu-Zr-Ag-Al glassy alloys with high GFA, Mater. Sci. Eng. B 148 (2008) 92–96, https://doi.org/10.1016/j.mseb.2007.09.064
[29] D. Turnbull, Under what conditions can a glass be found? Contemp. Phys. 10 (1969) 473–488, https://doi.org/10.1080/00107516908204405
[30] A. Takeuchi, N. Chen, T. Wada, Y. Yokoyama, H. Kato, A. Inoue, J.W. Yeh, Pd20Pt20Cu20Ni20P20 high-entropy alloy as a bulk metallic glass in the centimeter, Intermetallics 19 (2011) 1546–1554, https://doi.org/10.1016/j.intermet.2011.05.030
[31] S.F. Zhao, Y. Shao, X. Liu, N. Chen, H.Y. Ding, K.F. Yao, Pseudo-quinary $Ti_{20}ZrHf_{20}Be_{20}(Cu_{20-x}Ni_x)$ high entropy bulk metallic glasses with large glass forming ability, Mater. Des. 87 (2015) 625–631, https://doi.org/10.1016/j.matdes.2015.08.067
[32] M. Yang, X.J. Liu, H.H. Ruan, Y. Wu, H. Wang, Z.P. Lu, High thermal stability and sluggish crystallization kinetics of high-entropy bulk metallic glasses, J. Appl. Phys. 119 (2016) 245112, https://doi.org/10.1063/1.4955060
[33] H.Y. Ding, K.F. Yao, High entropy $Ti_{20}Zr_{20}Cu_{20}Ni_{20}Be_{20}$ bulk metallic glass, J. Non-Cryst. Solids 364 (2013) 9–12, https://doi.org/10.1016/j.jnoncrysol.2013.01.02
[34] T. Yamamoto, Y. Yokoyama, T. Ichitsubo, H. Kimura, E. Matsubara, A. Inoue, Precipitation of the ZrCu B2 phase in Zr50Cu50-xAlx (x=0,4,6) metallic glasses by rapidly heating and cooling, J. Mater. Res. 25 (2010) 793–800, https://doi.org/10.1557/JMR.2010.0105
[35] R. Busch, Y.J. Kim, W.L. Johnson, Thermodynamics and kinetics of the undercooled liquid and the glass transition of the $Zr_{41.2}Ti_{13.8}Cu_{12.5}Ni_{10.0}Be_{22.5}$ alloy, J. Appl. Phys. 77 (1995) 4039, https://doi.org/10.1063/1.359485
[36] Z.P. Lu, Y. Li, C.T. Liu, Glass-forming tendency of bulk La-Al-Ni-Cu-(Co) metallic glass-forming liquids, J. Appl. Phys. 93 (2003) 286, https://doi.org/10.1063/1.1528297
[37] M. Hillert, Phase Equilibria, Phase diagrams and phase transformations, Their Thermodynamic Basis, Second ed., Cambridge University Press, Cambridge, UK, 2008.
[38] D.R. Uhlmann, A kinetic treatment of glass formation, J. Non-Cryst. Solids 7 (1972) 337–348, https://doi.org/10.1016/0022-3093(72)90269-4
[39] H.A. Davies, Metallic glass formation, In Amorphous Metallic Alloys, ed. F.E. Luborsky, pp. 8–25. London, U.K.: Butterworths.
[40] R. Bohmer, K.L. Ngai, C.A. Angell, D.J. Plazek, Nonexponential relaxations in strong and fragile glass formers, J. Chem. Phys. 99 (1993) 4201, https://doi.org/10.1063/1.466117
[41] D.N. Perera, Compilation of the fragility parameters for several glass-forming metallic alloys, J. Phys. Condens. Matter 11 (1999) 3807–3812 https://doi:10.1088/0953-8984/11/19/303.
[42] R. Bruning, K. Samwer, Glass transition on long time scales, Phys. Rev. B 46 (1992) 11318–11322, https://doi.org/10.1103/PhysRevB.46.11318
[43] A. Jalali, M. Malekan, E.S. Park, R. Rashidi, A. Bahmani, Thermal behavior of newly developed Zr33Hf8Ti6Cu32Ni10Co5Al6 high-entropy bulk metallic glass, J. Alloy. Compd. 892 (2022) 162220, https://doi.org/10.1016/j.jallcom.2021.162220
[44] Y. Tong, J.C. Qiao, J.M. Pelletier, Y. Yao, Strong metallic glass: TiZrHfCuNiBe high entropy alloy, J. Alloy. Compd. 820 (2020) 153119, https://doi.org/10.1016/j.jallcom.2019.153119
[45] Y. Wang, Z. Zhu, A. Wang, H. Zhang, Ultrastrong behaviors of a non-equiatomic Ti-Zr-Ni-Cu-Be high entropy metallic glass with ultrahigh glass forming ability, J. Non Cryst. Solids 577 (2022) 121323, https://doi.org/10.1016/j.jnoncrysol.2021.121323